Proceedings of 14th IOE Graduate Conference
Peer Reviewed
Year: 2023 Month: December Volume: 14
ISSN: 2350-8914 (Online), 2350-8906 (Print)

Analysis of Bend Radius and Inlet Pipe Position on Hydronic Radiant Underfloor Heating System

Ishwor Acharya [a], Sanjeev Maharjan [b]

[a,b] *Department Of Mechanical and Aerospace Engineering, Pulchowk Campus, IOE, Tribhuvan University, Nepal*
[a] 076msmde008.ishwor@pcampus.edu.np

Abstract
With rising energy consumption for heating and cooling, there's a need to explore alternative technologies like floor heating systems (FHS). FHS offers cost-effectiveness, energy efficiency, and enhanced thermal comfort. This research focuses on a hydronic radiant underfloor heating system (RFHS) that employs water as a heat transfer medium for efficient heating in buildings. This study investigates the impact of bend radius and effect of inlet pipe position on temperature distribution across the floor surface for varying mass flow rates. The offset serpentine layout exhibited a larger temperature drop on the floor surface compared to the counterflow layout. A comparison of the two layouts revealed that the counterflow layout had lower pressure gradient and turbulent kinetic energy. The temperature near the bend region was influenced by the bend radius. Increasing the bend radius from 2mm to 30mm led to an increase in the temperature near the bend, while for bend radii above 40mm, the temperature near the bend region subsequently starts to decrease slightly. Altering inlet position in the counterflow layout, slightly elevated outlet temperature and overall floor temperature. This study contributes design guidelines for efficient FHS implementation.

Keywords
Thermal Comfort, Underfloor Heating, Temperature Distribution, Outlet Temperature

1. Introduction

Worldwide individuals and industries have enormous energy demand to power their homes, offices and to operate factories that produce substantial economic output. The buildings sector is a leading energy consumer which accounts for about 40% of the global energy consumption and contributes over 30% of the CO2 emissions [1]. Despite the prevailing global energy crisis, a large amount of energy is consumed annually to maintain thermal comfort within buildings [2]. Maintaining this standard of thermal comfort for occupants of buildings or other enclosures is one of the important goals for HVAC design engineers. About 10% of energy consumption at the household level in Nepal is used for the heating and cooling sector [3]. Hydronic RFHS work by circulating warm water through a network of pipes installed beneath the floor surface. These systems utilize the principle of radiant heat transfer, where heat is emitted from a network of pipes or electric heating elements installed beneath the floor surface, providing comfortable warmth to the room. These pipes are typically made of flexible, durable materials like cross-linked polyethylene (PEX) or polybutylene (PB). The pipes are laid out in a serpentine, counterflow pattern or in loops throughout the floor area, ensuring even heat distribution. The floor surface radiates the heat upward, warming the objects, occupants in the room and maintaining the desired temperature.

The main objective of this research is to analyze the bend radius and inlet pipe position on the hydronic radiant underfloor heating system. Studying the effects of various bend radii and inlet positions, this study seeks to develop guidelines and recommendations for designing and installing hydronic RFHS that optimize efficiency, ensure uniform heat distribution, and enhance overall performance. By investigating the effect of bend radius and inlet pipe position in hydronic radiant underfloor heating systems, this research aims to fill the existing knowledge gap and provide valuable insights for the design and optimization of these systems.

2. Design Assumption

The assumption and limitation of this research are listed as follows.

- Selective design parameters of the floor will be considered.
- Comparison of only three different piping layouts will be studied
- The research exclusively focuses on hydronic heating systems, while electrical resistance heating systems are not taken into consideration for analysis.
- Experimental validation of simulated results will not be performed
- The room is an enclosure that does not have doors, windows, and occupants.

3. Literature Review

RFHS has gained significant recognition as an effective and efficient method of heating in residential and commercial spaces. FHS maintains desired indoor temperature through heat transfer between the radiant surface and room by conduction, convection, and radiation [4]. The benefits of even heat distribution, energy efficiency, design flexibility, noise reduction and improved comfort have driven its adoption.

Under-floor heating is a system that utilizes pipes embedded in the floor to disperse heat both vertically and horizontally by circulating hot water [5]. In recent years, it has become increasingly popular in many countries and widely used in residential and public buildings. Economically, this system can provide heat at a reduced energy consumption rate, while also providing a higher level of control, efficiency, and quality [6]. Early research by Banerjee and Palmer [7] examined the effect of pipe spacing and insulation on the performance of radiant underfloor heating. and system performance. The study also highlighted the importance of insulation beneath the floor surface to minimize heat losses and improve system efficiency.

Gao et al. [8] conducted a study comparing five different under-floor heating pipe layout systems. The center spacing intervals ranged from 300 mm to 500 mm with a supply water temperature of 50 °C. The study examined the thermal homogeneity over the floor and the differences in vertical air temperature gradients.

The findings showed that the system provided a uniform indoor air temperature field above 0.1 m of the floor, with a temperature difference of no more than 1 °C. The study concluded that the optimal layout for the under-floor heating pipe is with a center spacing of 400 mm.

Liu and Li [9]did detailed investigation into the thermal performance and energy efficiency of two different piping layouts for underfloor heating systems: serpentine and counterflow configurations. The findings demonstrated that both layouts are capable of delivering efficient and effective heating to indoor spaces. The serpentine layout showed satisfactory thermal performance, effectively heating the floor surface and providing a comfortable indoor environment. On the other hand, the counterflow layout exhibited superior thermal performance compared to the serpentine layout. The numerical simulations revealed that the counterflow layout achieved more uniform heat distribution across the floor surface.

Numerous numerical and experimental studies were conducted over the past few decades to learn more about the thermal behavior of FHS. Ngo et al. [10] conducted a study which investigated the effect of design parameters on the performance of a radiant floor heating system. The experiment involved testing different pipe spacings (4 to 12 inches), depths (2.5 to 6.5 inches), and temperatures (45°C, 65°C, and 85°C) in three different mediums (air, gravel, and sand). The results showed that the most desirable floor temperature distribution was achieved with a shallow burial depth and closer pipe spacing. For instance, at a pipe spacing of 4 inches and depth of 2.5 inches, the floor surface temperature was relatively uniform, with a variation of only 1.6°C.The study also found that the average floor temperature was higher when the piping system was embedded in an air-filled space than in a porous medium such as gravel or sand.

Jin et al. [11] specifically focused on using the finite volume method to investigate the performance of a radiant floor cooling system by analyzing the impact of thermal resistance and water velocity. Their findings indicated that a lower thermal conductivity of the pipe is crucial for optimal system performance. Additionally, they found that water velocity has a minimal effect on the heat exchange between the water and the slab.

4. Research Methodology

4.1 Geometry design and Model Description

Three different piping layout offset serpentine, counter flow and counterflow with different inlet position were designed in the solid works. All three layout are designed on an 11.89m2 floor with dimensions 4.75m × 2.50m × 0.075m, is depicted in Figure 1 below. For offset serpentine the pipes feature 15 bends from the bottom to the top, positioned 12mm above the floor's bottom. The primary objective of this layout is to accommodate larger bend radii. Each pipe has a diameter of 13mm and is spaced at a distance of 150mm from the next. In total, 80m of pipe is used for all three model. The inlet and outlet are located at the bottom of the floor, spaced 150mm apart. The pipes are positioned 12mm above the floor's bottom and the bottom of the floor is equipped with 25mm of insulation. The inlet and outlet are located at the bottom of the floor, spaced 150mm apart. A total of 7 pipe circuits are used in counterflow layout, with a consistent spacing of 150mm throughout the floor surface.

The pipes are embedded 12mm above the bottom surface of the concrete floor, with a consistent spacing of 150mm throughout the floor surface. In the layout shown in figure c, the inlet is centrally positioned, at 1150mm from the bottom edge of the floor, with a spacing of 150mm from the outlet and the pipes run outward from the center. Here, the fluid initially flows towards the center of the floor, then moves outwards towards the corners of the floor, flows back towards the center, and eventually exits through the outlet.

4.2 Numerical Setup

For this study tetrahedral meshing was generated which involves dividing the 3D geometry into tetrahedral elements. In the offset serpentine layout, as depicted in Figure 2(a), a fine mesh with 4.5 million tetrahedral elements and 980,450 nodes was generated. The default target skewness of 0.9 was set to ensure mesh quality. For the counterflow layout, shown in Figure 2 (b), the meshing resulted in 4 million tetrahedral elements and 883,120 nodes. Likewise, for the counterflow layout with different inlet positions, as shown in Figure 2 (c), the meshing process produced 4.3 million tetrahedral elements and 890,386 nodes. The initial phase of the research involves simulating temperature distribution for offset serpentine and counterflow layout.

The second phase involves simulation counterflow layout with different bend radii for varying mass flow rate. The third phase involves simulating counterflow with different inlet position for varying mass flow rate. The simulations were conducted using Academic release of ANSYS Fluent 16.2, a software package for CFD analysis. The differential equation describing the principle of conservation of mass which is valid for incompressible and compressible flows are given in a general

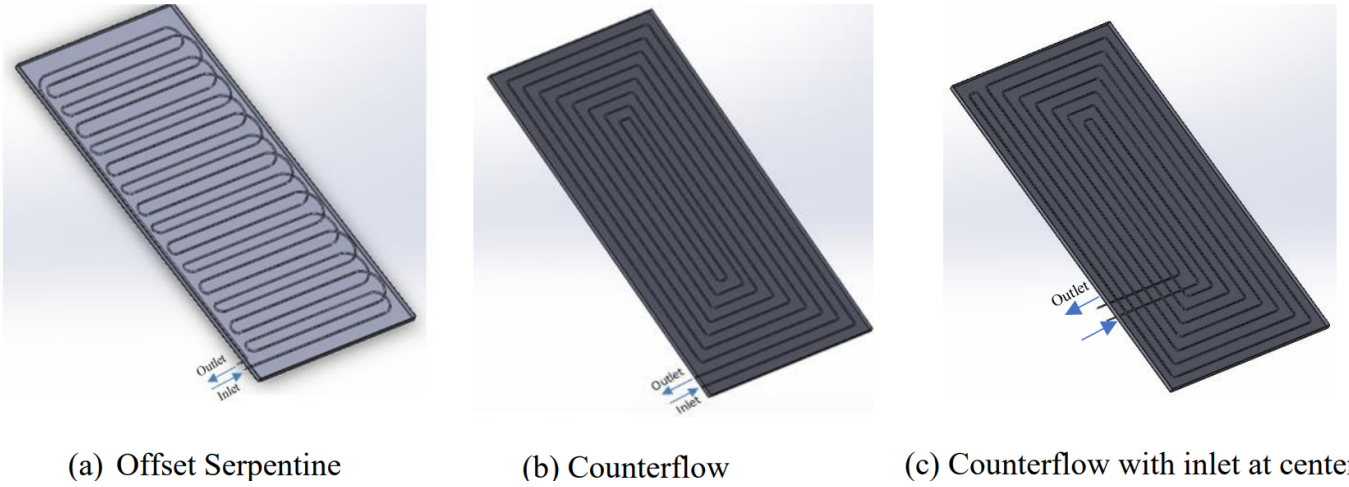

Figure 1: Three different piping layout of floor heating system

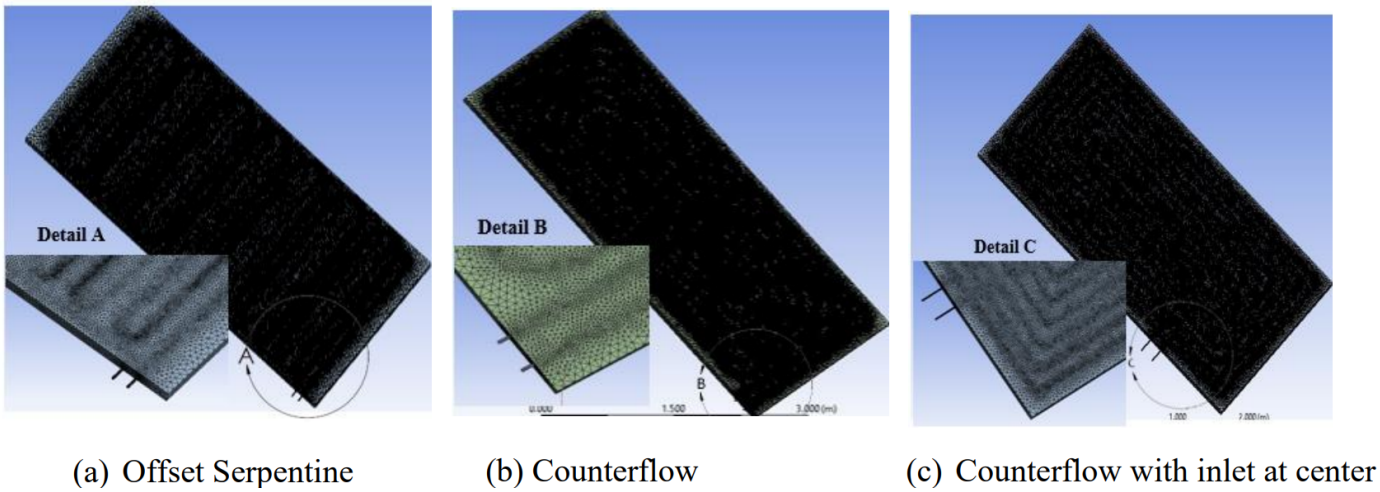

Figure 2: Mesh Structure of concrete and pipe for three layouts

Cartesian form below [12].

$$\frac{\delta \rho}{\delta t} + \frac{\delta}{dx_i}\left(\rho u_i\right) = 0 \tag{1}$$

Energy equation is given in Eq.(2)

$$\frac{\delta}{\delta t}(\rho E) + \frac{\delta}{\delta x_i}\left[ui(\rho E + P)\right] = \frac{\delta}{\delta x_j} k_{eff} \frac{\delta}{\delta x_i} + u_i(\tau_{ij})eff + S_h \tag{2}$$

Where P is the static pressure, $(\tau_{ij})eff$ is the stress tensor, the term $S_h$is the defined the source term given by the equation:

$$S_h = \frac{-U_g \times A \times (T_s - T_a)}{V_r} \tag{3}$$

E is total energy represented by:

$$E = h - \frac{P}{\rho} + \frac{u_i^2}{2} \tag{4}$$

The stress tensor, $(\tau_{ij})eff$ is given by the following correlation according

$$(\tau_{ij})eff = \mu_{eff}\left[\frac{\delta u_i}{\delta x_j} + \frac{\delta u_j}{\delta x_i}\right] - \frac{2}{3}\delta_{ij}\mu_{eff}\frac{\delta u_k}{\delta u_k} \tag{5}$$

where μ is the molecular viscosity, I is the unit tensor, and the second term on the right hand side is the effect of volume dilation.

The differential equation describing conservation of momentum for a Newtonian fluid flow is written:

$$\frac{\delta u}{\delta t} + u_i \frac{\delta u_i}{\delta x_i} = -\frac{1}{\rho}\frac{\delta P}{\delta x_i} + \frac{\delta}{\delta x_i}\left(\mu \frac{\delta u_i}{\delta x_j}\right) \tag{6}$$

To solve the governing equations numerically, the turbulence closure model used here is the standard K-ϵ to analyze turbulent properties of the flow. The floor surface average temperature is calculated by Eq. 7

$$T_s = \frac{1}{s}\int_0^s T_{i0}\,dx \tag{7}$$

The homogenization level of heat distribution on the floor surface is extremely important. A new parameter for characterizing this level is represented by

$$Tm = \frac{1}{\sum_c A_c}\left(\sum_c A_c T_c\right) \tag{8}$$

$$\sigma = \frac{1}{\sum_c A_c}, \left[\sum_c (A_c(Tc - T_m)^2)\right]^{1/2} \tag{9}$$

where A_c is the surface of element (m^2), T_c is the cell temperature (°C) and T_m is the mean temperature (°C). The high values of σ indicate that there is a high heterogeneity of temperature at the floor surface.

In this case, the domain of solution includes two different components; concrete block and the fluid system. The calculations were performed using second order upwind discretization scheme using SIMPLE algorithm. The convergence criteria were set to 10^{-4}.

Table 1: Boundary Condition

Layout	Location	Value
Offset serpentine / Counterflow	Inlet mass flow	0.23 Lps
	Inlet temperature	323K
	Outlet	Pressure Outlet
	Wall-fluid domain interface	Coupled
	Freestream temperature	297K
	Convection coefficient of air	10 W/m^2k
	Floor Bottom	Insulated

5. Results and Discussion

5.1 Temperature distribution for offset serpentine and counterflow layout

The temperature distribution for Offset Serpentine and counterflow layout is shown in Figure 3. As shown in Figure 3(a) for offset serpentine layout it is observed that a low-temperature region forms on the floor surface as the water flows towards the outlet. When the mass flow rate is 0.23 Lps, the overall floor temperature near the surface is around 307K. Temperature drops are seen near the bend region, particularly above the mid region of the floor. At the mid region, the temperature is around 305K, and it spreads to a larger area as the fluid passes to the top of the floor. The temperature difference between the entry and exit of the loop is approximately 8K.

For this layout the temperature is evenly distributed across the floor surface. In Figure 3 (b), with a mass flow of 0.23 lps, the temperature near the bend drops by about 1.5K, while the overall floor surface temperature is approximately 309K. The temperature difference between the entry and exit of the loop is about 5K. In Figure 3 (c), when the mass flow is reduced to half (0.12lps), the overall floor temperature remains at 307K throughout the floor surface, and near the bend region, it drops to 305.36K. Cold spots start to form near the bend and become more prominent with reduced flow rate.

5.2 Temperature near bend for counterflow layout with various bend radius and mass flow rate

The graph in Figure 4 below presents the temperature variations near the bend for a counterflow layout with different bend radii (2mm, 20mm, 30mm, 40mm, 50mm, 65mm, 190mm) and three distinct mass flow rates (0.23lps, 0.12lps, and 0.06lps).

The temperature distribution for various bend radius with different mass flow is shown in Table 6. Analyzing the chart reveals the significant influence of inlet mass flow rate and bend radius on the temperature distribution along the bend. It is seen that the temperature near the bend region is affected by the bend radius. For a constant pipe spacing as the bend radius is increased the temperature starts to drops gradually near the bend. As seen on graph, for a mass flow of 0.23Lps and bend radius 2mm the bend temperature was 306K. As the bend radius increases to 30mm, the temperature near the bend reaches its peak and subsequently starts to decrease slightly. Beyond a bend radius of 40mm, it becomes evident that the temperature near the bend region gradually decreases for all three mass flow rates. When examining the effect of mass flow rates, it was observed that a larger mass flow rate (0.23lps) led to a smaller temperature drop of approximately 0.2K with changes in bend radius.

In contrast, a sudden drop-in mass flow rate (0.06lps) resulted in a more significant temperature drop of over 0.4K. The temperature drop near the bend was larger for large bend with decrease in mass flow rate.

5.3 Analyze the effect of inlet pipe position on temperature distribution for counterflow layout for different mass flow rate

The temperature distribution on the floor surface for the counterflow layout with a change in inlet position is shown in Figure 5. The analysis is conducted for 3 different mass flow rates: 0.23lps, 0.12lps, and 0.06lps, respectively. At a mass flow rate of 0.23lps as shown in Figure 5(a), the overall temperature distribution throughout the floor surface was uniform at 310K. The floor corners formed a low-temperature. region of 305K, and no temperature drop was observed near the bend region. The temperature on the floor surface near the wall region was about 309K. The outlet temperature for this piping layout is 320K, and there is a difference of 3K between the entry and outlet temperatures.

As shown in Figure 5 (b) the mass flow rate was reduced to half 0.12lps and the temperature distribution on the floor surface was observed. The overall floor surface temperature was 308K, and the wall corners developed a low-temperature region. Additionally, it was noticed that a few bend regions near the corners had a low-temperature zone of 305K. The reduced mass flow resulted in the growth of a low-temperature zone near the floor walls and also near the outlet region. As shown in Figure 5 (c) the mass flow rate was further reduced to 0.06 lps and the temperature distribution on the floor surface was observed. The overall floor surface temperature was 305K, and the outlet temperature was 316K. As we reduced the mass flow rate, we observed the formation of a few low-temperature regions of 302K near the bend region on the floor corners. The temperature near the floor walls grew larger in size, and a temperature drop of 302K near the inlet and outlet regions was noticed. However, no temperature drop was observed near the bend in the central region. The reduction in mass flow rate resulted in a few cold spots of 297K near the floor wall.

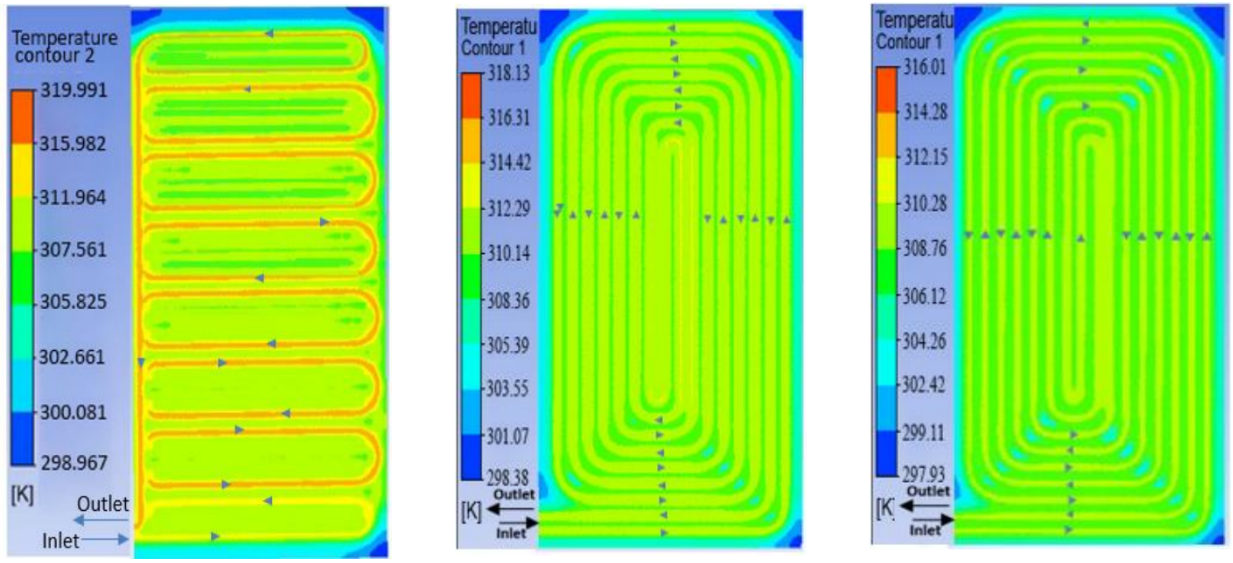

(a) Offset serpentine at 0.23lps (b) Counterflow at 0.23lps c) Counterflow at 0.12lps

Figure 3: Temperature distribution for offset serpentine and counterflow layout

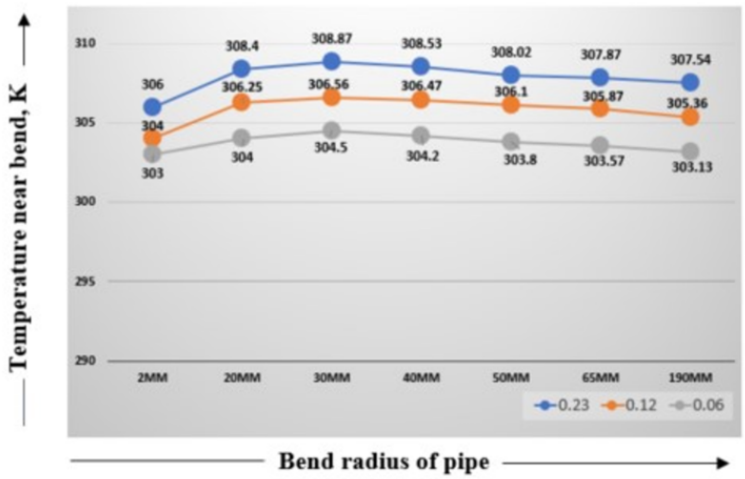

Figure 4: Temperature near bend for various bend radius and mass flow rate

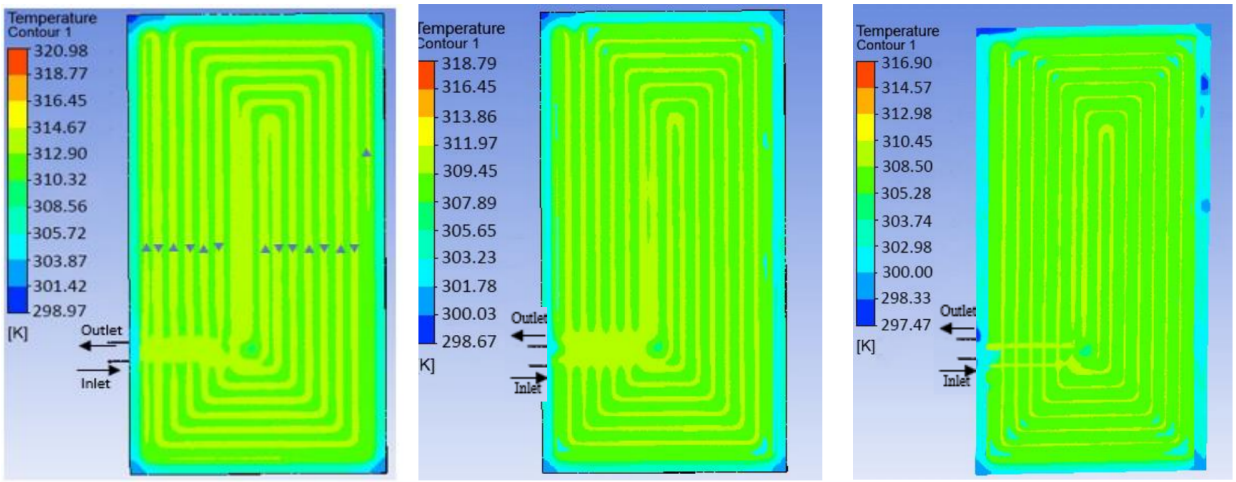

(a) 0.23 Lps mass flow (b) 0.12 Lps massflow (c) 0.06 Lps mass flow

Figure 5: Temperature profile for counterflow with change in inlet pipe position

Bend Radius	Massflow 0.23 lps	Massflow 0.12 lps	Massflow 0.06 lps
2mm	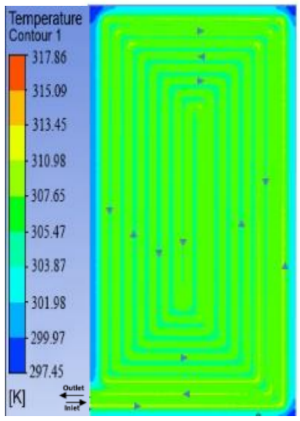	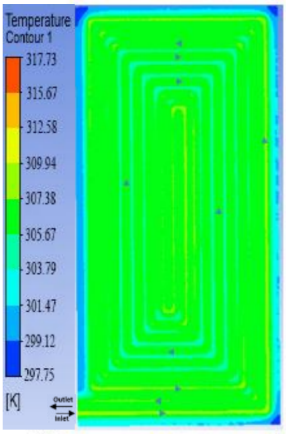	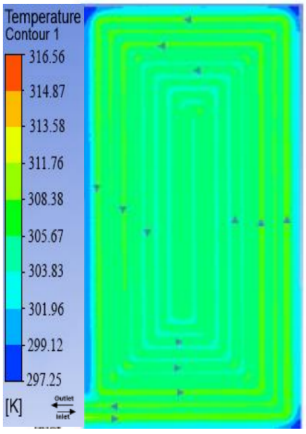
30mm	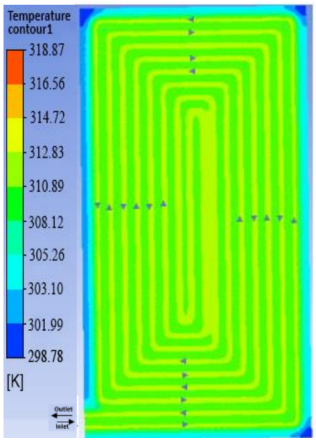	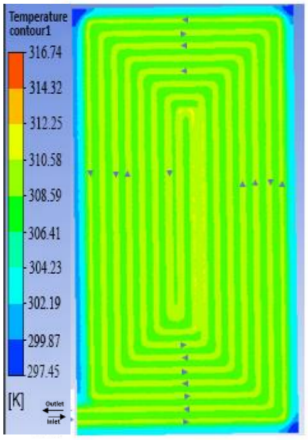	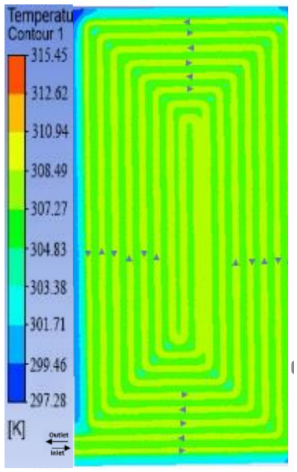
65mm	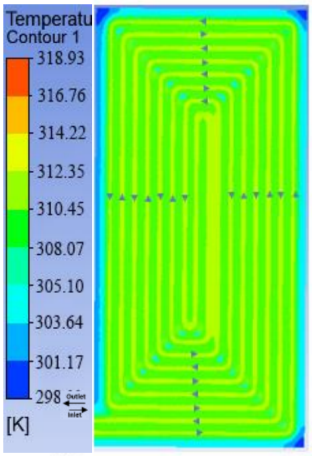	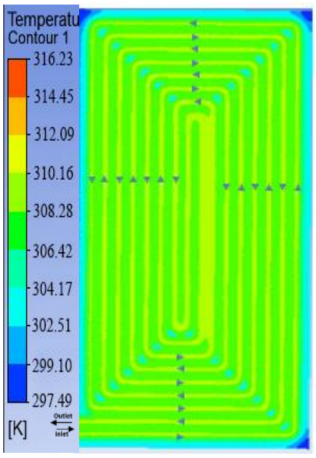	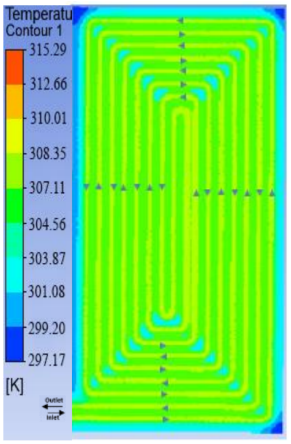
190mm	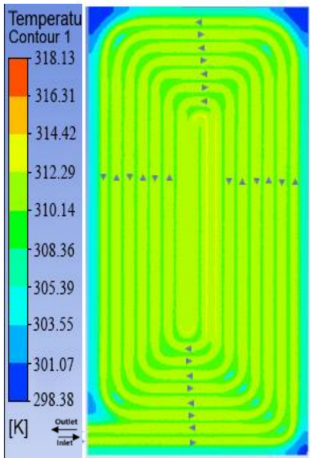	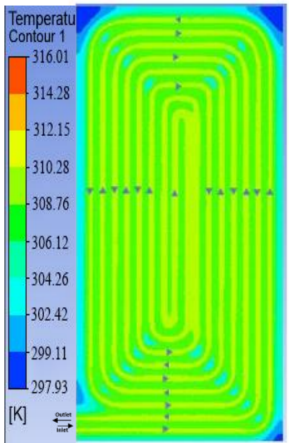	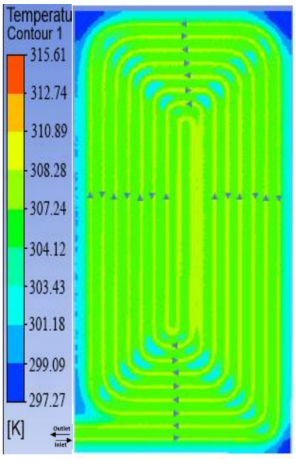

Figure 6: Temperature distribution near the bend for counterflow layout with bend radii 2mm, 30mm, 65mm and 190mm

5.4 Validation of Results

To validate the findings of this study, comparisons were made with relevant research in the field. In a study conducted by SK Mishra [13], a similar investigation into temperature distribution was undertaken, focusing on counterflow and serpentine layout configurations.Both serpentine and the offset serpentine layouts demonstrated non-uniform temperature distributions on the floor surface.The offset serpentine layout had a temperature gradient of 8K, while 5K gradient was observed in Mishra serpentine layout. Similarly, both counterflow layout exhibited uniform temperature distribution while the temperature gradient was found to be larger for our layout by 4K and the overall floor temperature was also higher.Temperture drop was observed near the bend region for both layout.Coldspots were formed near the pipe bends with increase in pipe spacing and bend radius.

While Mishra recommended larger bend radii during installation,however our analysis found that larger bend radii actually increased the cold region near the bends. It was observed that the optimum bend radius for reducing cold spots was in the range of 30-40mm.

6. Conclusion

The offset serpentine layout exhibited a larger temperature drop on the floor surface compared to the counterflow layout. The temperature at the outlet for the counterflow model was approximately 3K higher than that of the offset serpentine layout. For offset serpentine layout temperatures dropped noticeably near the bend region above the mid-region, on the other hand, the counterflow layout exhibited a more uniform temperature distribution across the entire floor surface, showing consistent heat transfer characteristics. Furthermore, for bend radii beyond 40mm, the temperature near the bend showed a gradual decrease for all three tested mass flow rates. Overall, the study revealed that larger bend radii contributed to more substantial temperature drops near the bends, particularly when combined with decreased mass flow rates. The fluid flow was reversed, circulating from the floor center to the outer edges. This change in inlet position resulted in the fluid being preheated to some extent before reaching the central region. As a result, at a mass flow rate of 0.23lps, the temperature at the outlet was slightly higher, reaching 320K, and the overall temperature on the floor surface reached 310K.

References

[1] Liu Yang, Haiyan Yan, and Joseph C Lam. Thermal comfort and building energy consumption implications–a review. *Applied energy*, 115:164–173, 2014.

[2] Harimi Djamila. Indoor thermal comfort predictions: Selected issues and trends. *Renewable and Sustainable Energy Reviews*, 74:569–580, 2017.

[3] Sudhir Man Shrestha. Energy efficient building for nepalese market. Master's thesis, UiT Norges arktiske universitet, 2017.

[4] H Khorasanizadeh, GA Sheikhzadeh, AA Azemati, and B Shirkavand Hadavand. Numerical study of air flow and heat transfer in a two-dimensional enclosure with floor heating. *Energy and buildings*, 78:98–104, 2014.

[5] Hasan Karabay, Müslüm Arıcı, and Murat Sandık. A numerical investigation of fluid flow and heat transfer inside a room for floor heating and wall heating systems. *Energy and Buildings*, 67:471–478, 2013.

[6] Xiaozhou Wu, Jianing Zhao, Bjarne W Olesen, Lei Fang, and Fenghao Wang. A new simplified model to calculate surface temperature and heat transfer of radiant floor heating and cooling systems. *Energy and buildings*, 105:285–293, 2015.

[7] P. K. Banerjee and M. Palmer. Experimental study of a radiant floor heating system. solar energy. 47:111–119, 1991.

[8] J. Gao, H. Chen, , and S Xiong. A review of hvac technologies for energy efficient buildings. *Applied Energy*, 204:1161–1174, 2017.

[9] T. Liu and B Li. Experimental study on radiant floor heating system. pages 465–471, 2015.

[10] CC Ngo, BA Alhabeeb, and M Balestrieri. Performance comparison of serpentine and counterflow layouts for underfloor heating systems using cfd simulations. 57496:V08AT10A050, 2015.

[11] Xing Jin, Xiaosong Zhang, Yajun Luo, and Rongquan Cao. Numerical simulation of radiant floor cooling system: The effects of thermal resistance of pipe and water velocity on the performance. *Building and Environment*, 45(11):2545–2552, 2010.

[12] Muhammad Ahsan. Numerical analysis of friction factor for a fully developed turbulent flow using k–ε turbulence model with enhanced wall treatment. *Beni-Suef University journal of basic and applied sciences*, 3(4):269–277, 2014.

[13] Mishra S.K. Design and analysis of solar under floor heating system. *Tribhuvan University,IOE*, 2017.